Eur. Phys. J. C (2024) 84:181
https://doi.org/10.1140/epjc/s10052-024-12528-9

THE EUROPEAN PHYSICAL JOURNAL C

Check for updates

Regular Article - Theoretical Physics

Investigation of scalar and fermion dark matter in mono-photon production at high-energy colliders

G. Gil da Silveira[1,2,a], **M. S. Mateus Jr.**[2,b]

[1] PH Department, CERN, 1211 Geneva, Switzerland
[2] Group of Analysis and Simulation of Particles (GASP), IF-UFRGS, Caixa Postal 15051, Porto Alegre, RS CEP 91501-970, Brazil

Received: 8 July 2023 / Accepted: 7 February 2024 / Published online: 22 February 2024
© The Author(s) 2024

Abstract Many theories about dark matter have emerged due to its strong theoretical appeal in explaining astrophysical phenomena. However, experimental and theoretical particle physics have yet not provided evidence that dark matter is part of the observable Universe. Our work aims to investigate the interaction between Standard Model (SM) fermions and different species of dark matter (DM) particles in high-energy collisions through interaction of a new massive vector mediator, Z'. The production of scalar and fermion DM pairs via fermion annihilation into the new vector boson is investigated near a resonance ($m_\chi \sim M_{Z'}/2$), where a SM signal from hard photon emission is considered as initial state radiation, namely a mono-photon production. Values of coupling constants between the DM and the SM particles are mapped in contrast to the Planck satellite data for thermal relic density DM computed in the correct framework for the relic density near a resonance, where a weaker suppression of the relic density is expected. We show for the CLIC and LHC kinematic regimes that certain mass ranges and coupling constants of these DM particles are in agreement with the expected relic density near a resonance and are not excluded by collider and astrophysical limits.

1 Introduction

The Standard Model (SM) of the elementary particle interactions has been tested for a variety of phenomena in particle physics at great precision. Nevertheless, there is no (currently) particle in the SM that satisfies the characteristics of the dark matter (DM), i.e., a suitable candidate to explain astrophysical phenomena at cosmological, galaxy cluster and galactic scales. Neutrinos, for example, known to have non-zero mass [1], would be an ideal candidate for DM, however their mass is too small to account for large structure formation [2,3]. It is reasonable, therefore, to conceive extensions of the SM that could include new particles and interactions that are consistent with an even more complete description of nature. Several studies have been proposed to investigate the DM and to decipher its origin and nature [2–9], where distinct approaches aim to understand how DM interacts, with itself and with the SM particles, and what could be the possible mechanisms of detecting it.

Following Refs. [3,10–12], our work assumes a simplified model where the interaction of any Weakly Interactive Massive Particle (WIMP) with the SM is mediated by a new massive boson at GeV–TeV scale, which we will indicate hereafter by Z' [12–15]. This Z' boson then acts as a mediator in the production of primordial DM until the *freeze-out* is reached [16]. A higher mass mediator is preferred due to strong experimental constraints in the search for a resonance at lower masses, then we show that a massive vector mediator on the TeV scale would be accessible even with the restrictions imposed on phase space by the current collider searches. Unlike the cases analyzed in Refs. [10,11], we do not assume a priori any effective model and proceed with the calculation of the total cross section, σ_{tot}, using the Feynman rules obtained from the simplified model Lagrangian, where the templates for couplings and vertices remain very similar to those in the SM for massive gauge bosons. Hence, we are not only interested in parameters related to the final state of the particles, such as their mass and spin, but also on the characteristics for a mediator Z' and their couplings with the initial state fermions, ψ, and the DM particle, χ, in final state.

In this context, we could attempt to recreate it with the use of particle colliders with sufficient high energies if DM was produced by a thermal process that has gone through a freeze-out [16]. An arbitrary coupling of DM with ordinary

[a] e-mail: gustavo.silveira@cern.ch (corresponding author)
[b] e-mail: msmateusjr@gmail.com

matter is hence assumed, expressed in the form of an arbitrary gauge coupling, which would represent a direct dark sector coupling to leptons and/or quarks [3,17–19]. Nonetheless, the detection of DM particles poses a major experimental challenge, since DM-related couplings are expected to be very weak [20], e.g., as much or even more than those with neutrinos, and exclusion limits have been recently imposed on massive vector mediators up to the TeV scale [21–23]. In general, searches in high-energy colliders focus in the observation of DM signatures in the form of missing transverse momentum or missing transverse energy [24–26]. Such a signal would occur if the DM particles are invisible to the detector or a possible charged DM particle has a sufficiently long lifetime to pass through the detector volume and leave a characteristic trace of charged particles, decaying shortly into particles too light to generate any signs on the detector calorimeters.

In this work we investigate the Z' production via monophoton production process in electron-positron annihilation (e^+e^-) at CLIC at $\sqrt{s} = 3$ TeV [27] and for proton-proton (pp) collisions at the LHC at $\sqrt{s} = 14$ TeV in the scenario where the invisible decay products of the Z' mediator, i.e. DM particles, have invariant masses close to the resonance and the photon is the SM signal to be triggered. Considering the limits already imposed by the searches performed by the ATLAS and the CMS Collaboration of DM mediator mass above 2 TeV [28,29], we focus this study in a Z' mass of 3 TeV in both CLIC and LHC. As a result, one has to properly account for the viability of the DM model candidate by accounting for the expected relic density, and this calculation cannot rely on the usual framework usually done away from resonances. As shown in Refs. [30,31], the proper treatment of the relic density near a resonance results in a weaker reduction of the expected relic density. Hence, we compare our predictions for the production cross sections with the proper evaluation of the relic density for DM species for the first time in the literature.

This paper is organized as follows: in Sect. 2 we describe the theoretical modeling of the Z' mediator, with some motivations for a scalar and fermion final DM states,[1] nonetheless a richer dark sector can be studied in the TeV scale in a subsequent analysis, as proposed by [33]. In Sect. 3 we present the evaluation of the relic density near a resonance. This approach enables effective comparisons with results in the literature typically obtained without taking the resonance into account. In Sect. 4 we discuss how this model could be perceived with a ISR assuming a hard-photon emitted by the an incoming fermion [34] and present the results obtained for the mass and coupling constant regions available at the high-energy CLIC and LHC colliders. Finally, we present our conclusions in Sect. 5.

2 Theoretical framework

Extensions of the SM can usually be studied using effective, simplified, or (so to say) complete models [1,3]. Still, we can make several claims regarding the nature of the kind of New Physics we expect to find even with the simplest effective models [35]. These models are a starting point for studying New Physics, given their simplicity on describing the particles and interactions involved using only a small number of parameters that can be directly related to experimental observations, such as: mass of the particles involved, their decay widths, production cross sections of these new processes, among others [36]. One can apply a simplified model in trying to explain some New Physics results through functions of the variables involved in its description, excluding certain values based on different experimental constraints [37].

We start with interaction Lagrangians describing a SM extension with some new symmetry group $U_\chi(1)$ acting as a vector portal for DM. The use of a $U_\chi(1)$ symmetry for investigating interactions between DM and SM has been widely proposed [1,17,38,39] and very tightly constrained at low and high masses have been imposed mostly by collider experiments (e.g., see Refs. [28,29]). This work explores a framework to probe the limits and to analyze parameters for the DM thermal production through a process that involves interactions of the SM with the dark sector mediated by a new massive boson mediator (Z') described with a Breit–Wigner (BW) resonance. Such mediator couples to scalar and fermion fields as candidates for DM. Feynman diagrams representing the s-channel Z'_μ exchange with DM candidates, χ, are shown in Fig. 1, where $g_{r/l}$ and g_χ are the couplings of this new spin-1 boson to the SM and the different DM fields, respectively. Here we investigate the different final DM states as separated cases; details of the implications of the simultaneous existence of these final states for DM and possible interactions between them are beyond the scope of this work. These possible states would be an aspect of a even more complete model where further studies could be performed with a experimental observation. We then focus on the evaluation of the cross section and in turn analyze the parameter space more comprehensively. As widely followed in the literature, we do not focus on how the Z' boson acquires its mass, nor we delve into details regarding the gauge regularization of the presented Lagrangians, which does not hinder the derivation of our results or similar studies [40] that follows this same methodology. More comprehensive models on spin-1 mediators and the related final states that prescribe their gauge

[1] Here we assume that each kind of DM final state composes all the DM relic abundance observed by the PLANCK satellite [32].

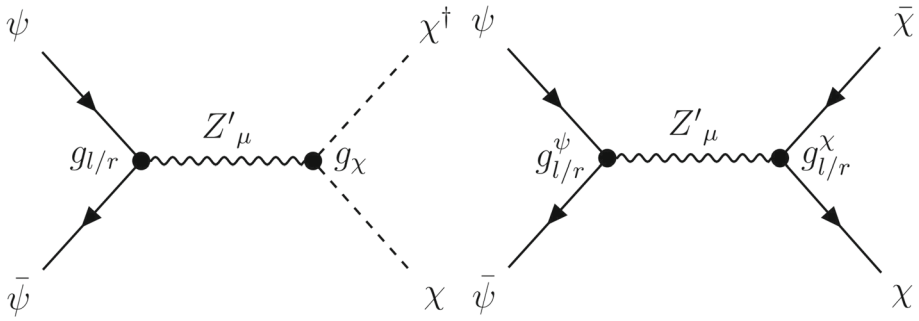

Fig. 1 Feynman diagrams for the interaction of SM fermions, ψ, with a scalar (left), fermion (right) χ, field through a Z' boson. The couplings $g_{r/l}$ and g_χ represents the coupling of the Z' boson with the SM and the DM fields, respectively

invariance are described in Refs. [1,2,9,12,17,29,38,41–44].

2.1 Tree-level process with s-channel resonance

Let ψ be any SM fermion spinor and Z'_μ a real vector[2] field corresponding to an on-shell massive spin-1 mediator coupling to scalar particles representing the DM fields [Fig. 1 (left)]. An extension interaction Lagrangian of this process can be written as

$$\mathcal{L}_{\text{int}}^{\text{scalar}} \supset \bar{\psi}\gamma^\mu \left(g_l P_L + g_r P_R\right) \psi Z'_\mu + g_\chi \left(\chi^\dagger \partial_\mu \chi - \chi \partial_\mu \chi^\dagger\right) Z'^\mu, \tag{1}$$

where we use $M_{Z'}$ for the mediator mass and γ^μ are the usual Dirac matrices. The P_L and P_R operators refer to left and right-handed operators, respectively, defined by $P_L \equiv \frac{1}{2}(1-\gamma^5)$ and $P_R \equiv \frac{1}{2}(1+\gamma^5)$, with g_l and g_r representing chiral coupling magnitudes. The final DM scalar state is well motivated both in simplified effective models and more complete models containing sometimes a Higgs doublet [9,41,42] that can act as a mediator between or be the main composition of a dark sector. In most of the literature, masses below a few GeV are largely excluded by different experimental DM detection pathways [45–47], hence we discuss the production of scalar DM where the final state mass is on the TeV scale.

For a DM particle characterized as a Majorana fermion (Fig. 1, right), the interaction Lagrangian has the form

$$\mathcal{L}_{\text{int}}^{\text{fermion}} \supset \left[\bar{\psi}\gamma^\mu \left(g_l P_L + g_r P_R\right) \psi + \bar{\chi}\gamma^\mu \left(g_\chi P_L + g_\chi P_R\right) \chi\right] Z'_\mu, \tag{2}$$

where we adopt $g_{l/r} \neq g_\chi$ and $g_{\chi,r} = g_{\chi,l} = g_\chi$ due to the Majorana condition for the spinor components. Moreover, we see that the interaction of the Z' boson with the DM field is given by the operators in the last term of Eq. 2, which also contains the adjoint spinor for the DM particle $\bar{\chi}$ and once again the chiral operators and couplings.

[2] Depending on the chosen coupling configuration, this mediator can function as an (axial)vector or a chiral vector. Refer to Table 1 for further details.

Fermion DM is well motivated through the literature and seen as one of the main candidates for WIMP DM in many different models [1,2,29,38]. For instance, a well-studied case in minimal supersymmetric models (MSSM) [48] would be the existence of a long lived particle (LLP) in the form of a neutralino, Dirac or Majorana fermion coming from the symmetry of the neutral mediators of the SM. However, in the case of the LLP, as well as other candidates, the manifestation in any experiments would not necessarily classify this new particle as dark matter itself. Further investigations would be required to identify its properties to trace it as new physics that explains any of the open problems in contemporary physics, including the issue of dark matter in astrophysical observations [12,29]. Furthermore, universal extra-dimensional models [43] as well as models with sterile neutrino [44] introduce candidates in the form of a fermion final state, sometimes discussed in another mass scale though. We emphasize that we deal with masses at the TeV scale, an accessible mass window in searches at high-energy collider experiments.

2.2 Production cross section and decay widths

The cross sections for all process in Fig. 1 are obtained with the help of `FeynCalc` [49] and `FeynArts` [50] packages available for the `Wolfram Mathematica` software [51]. From the Lagrangians and Feynman diagrams, scattering amplitudes are obtained and evaluated using Feynman rules and appropriate kinematic variables for these packages. Once the expression for the total cross section of the process $2 \to 2$ is obtained, the mass and couplings of the particles involved in the process are treated as free parameters and evaluated separately.

The total cross section, $\hat{\sigma}_{\text{tot}}$, for a process $2 \to 2$ in the center-of-momentum (CM) frame can be calculated in terms of the Mandelstam variable s, averaging over the spin of the initial states of those processes and the square of weighted scattering amplitude over all initial spin states. Thus we obtain the total cross section for these processes:

Table 1 Categorization of SM couplings following the definition given in Ref. [10]

Coupling type	Definition
Vector	$g_l = g_r$
Axial-vector	$g_l = -g_r$
Right (*chiral*)	$g_l = 0$

$$\hat{\sigma}_{\text{tot}}^{\text{scalar}} = \frac{g_\chi^2 \left(g_l^2 + g_r^2\right)\left[s(s-4m_\chi^2)\right]^{3/2}}{192\pi s^2\left[\left(s-M_{Z'}^2\right)^2 + \Gamma^2 M_{Z'}^2\right]}, \tag{3a}$$

$$\hat{\sigma}_{\text{tot}}^{\text{fermion}} = \frac{g_\chi^2\sqrt{s-4m_\chi^2}\left[g_l^2\left(s-m_\chi^2\right) + 6g_l g_r m_\chi^2 + g_r^2\left(s-m_\chi^2\right)\right]}{48\pi\sqrt{s}\left[\left(s-M_{Z'}^2\right)^2 + \Gamma^2 M_{Z'}^2\right]}. \tag{3b}$$

The terms for the BW width ($\Gamma^2 M_{Z'}^2$) in the denominator of the scattering amplitudes correspond to the mediator exchange of a s-channel resonance.

As we will deal with the cross section of a process involving a massive spin-1 mediator, we need to compute the decay widths. The Z' decay into both species of DM particles are evaluated to determine the decay width, Γ^{i}, at which it can decay into two DM particles of identical masses m_χ. The calculation is performed in the same way as for any $1 \to 2+3$ process, where the decay width Γ takes the form:

$$\Gamma_{a\to b+c} = \frac{|\vec{p}_f|}{8\pi M^2}\frac{|\mathcal{M}_{1\to 2}|^2}{3}, \tag{4}$$

resulting in the respective decays widths for each DM final state:

$$\Gamma^{\text{scalar}} = \frac{g_\chi^2\left(M_{Z'}^2 - 4m_\chi^2\right)\sqrt{1-4m_\chi^2/M_{Z'}^2}}{48\pi M_{Z'}}, \tag{5}$$

$$\Gamma^{\text{fermion}} = \frac{N_f\left[g_{l\chi}^2\left(M_{Z'}^2 - m_\chi^2\right) + 6g_{l\chi}g_{r\chi}m_\chi^2 + g_{r\chi}^2\left(M_{Z'}^2 - m_\chi^2\right)\right]\sqrt{1-4m_\chi^2/M_{Z'}^2}}{24\pi M_{Z'}}. \tag{6}$$

In this context, the parameter N_f represents the count of fermions with which Z' can decay within the SM sector. Specifically, we set $N_f = 6$ for e^+e^- collisions, where Z' exclusively couples with leptons, and $N_f = 18$ when Z' couples solely with quarks. We can separate the SM coupling in different types due to the nature of the mediator. From left and right projection operators, the Z' mediator can be vector, axial-vector, or chiral, with coupling constants according to Table 1, where we use $g_{l\chi} = g_{r\chi} = 1$ in the fermion case [10].

2.3 Initial-state photon radiation

The experimental detection of DM is a hard task given the unknown characteristics of its interaction with ordinary matter, hence ways of detecting it is a topic of intense research [52], typically leading to the search of events with missing transverse energy (MET), $\vec{E}_T$. One way of observing a DM event with MET is to consider the emission of SM particles as initial state radiation (ISR). As such, different particles can be emitted from the initial colliding particles, collectively known as mono-X searches. The search for a photon as ISR is natural as electromagnetic radiation is perhaps one of the simplest to be measured with precision at experiments in particle colliders. Also, it can have a very broad spectrum, on scales from keV to TeV, depending on the invisible event that one want to characterize [39,53–55].

Radiative corrections to the tree-level DM process are necessary to account for DM production via mono-photon process. While most of the studies in the literature are given in terms of an approximation with a soft photon or calculated numerically for a $3 \to 2$ process [56–58], we choose here to account for the radiative correction with emission of a hard photon as discussed in the classical approach by Ref. [34] which also were used in subsequent works [59–63] in non-exclusive DM contexts. This framework proposes a factorization in terms of lower order processes where $\psi\bar{\psi}$ reactions generate a final state with the emission of a hard photon in the event. This particular approach uses a rigorous calculation of higher order corrections together with a more precise evaluation of the phase space of the emitted photon. Such precautions are necessary due to the high energy involved and the emitted photon itself, which would disqualify a process containing only one ISR of a low energy or soft collinear photon, as in the Weizsäcker–Williams (WW) approximation [10,64]. We employ this framework by using the appropriate factorization to obtain the total cross section

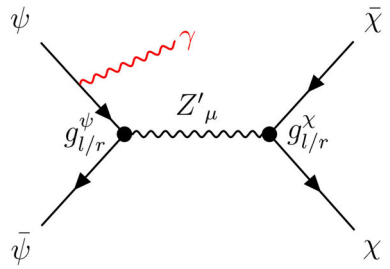

Fig. 2 A representation of a Feynman diagram with the emission of a photon as ISR, in red wiggly line, in the case of fermion DM production

for a mono-photon process, as represented in Fig. 2:

$$\sigma'_{\rm tot}(\psi\bar{\psi} \to Z'\gamma \to \gamma\chi\bar{\chi}) = \hat{\sigma}_{\rm tot}(\psi\bar{\psi} \to Z' \to \chi\bar{\chi})(1+\delta), \tag{7}$$

with $\hat{\sigma}$ given by Eq. 3 integrated over the scattering amplitude squared for each DM species and

$$\delta = \frac{2\alpha}{\pi}\left\{\left(-1+2\log\frac{\sqrt{\hat{s}}}{m_\psi}\right)\left[\log x_\gamma^{\rm min} + \frac{13}{12} + \int_{x_\gamma^{\rm min}}^{x_\gamma^{\rm max}} {\rm d}x_\gamma\, \xi(x_\gamma)\right] - \frac{17}{36} + \frac{\pi^2}{6}\right\}, \tag{8}$$

$$\xi(x_\gamma) = \frac{1}{x_\gamma}\left(1 - x_\gamma + \frac{x_\gamma^2}{2}\right)\frac{\hat{\sigma}(\hat{s}-\hat{s}x_\gamma)}{\hat{\sigma}(\hat{s})}, \tag{9}$$

where $\alpha = 1/137$ is the electromagnetic fine structure constant, q_γ is the momentum carried by the photon from ISR, and $\hat{\sigma}(\sqrt{\hat{s}})$ is the total cross section of the $2 \to 2$ process, with energy $\sqrt{\hat{s}}$. Function $\xi(x_\gamma)$ takes into account the available center-of-mass energy for producing the DM pair plus a hard photon, which decreases for more energetic photons. This can be seen in Fig. 3 (top panel) where the function $\xi(x_\gamma)$ is shown, which depends on the partonic cross section with and without ISR, for all DM species. The shape of the distribution is very similar for all mediator couplings, although the fermion DM a little enhancement in the tail towards high x_γ. A typical photon spectrum in particle detectors starts at a few GeV where isolation and reconstruction efficiencies are above 90%.

Considering a usual efficiency turn-on curve in trigger selection, we employ $x_\gamma = q_\gamma/E_{beam}$ with a minimum photon energy of 60 GeV, or $x_\gamma = 0.04$ for a beam of 1.5 TeV, motivated by the identification capabilities expected at CLIC dp [65] and assessed in the LHC experiments [66]. Figure 3 (bottom panel) shows the distribution of the ratio between the total cross sections with and without ISR in terms of the minimum photon energy $x_\gamma^{\rm min}$, which illustrate the contribution of the δ term in Eq. 7. Although the shape of $\xi(x_\gamma)$ decreases rapidly with increasing photon energy fraction, the radiative corrections improve the production cross section at higher photon energies up to $\sim 7\%$, which is independent of the dark sector parameters, such as masses and coupling constants. Also, the dip structure occurring around $x_\gamma^{\rm min} \approx 0.02$ reveals the effect of the corrections for very low photon energies. The ratio reaches a value of 1 at $x_\gamma^{\rm min} \approx 0.06$, marking the starting point at which the radiative corrections enhance the total cross-section. Although the chosen value of 0.04 as minimum photon energy in this study is located in a region where the cross section is slightly suppressed, we aim to investigate the kinematic region expected for the photon identification in experiments, especially at CLIC dp.

As shown in Ref. [67], the production cross section of DM pairs plus hard photon are $\mathcal{O}$(fb), making its observation possible with an integrated luminosity of the order of ab^{-1}. Similar simulations also indicate high visibility in the emission and consequent detection of mono-photons from invisible decays, with significant cross section and transverse momentum fraction of the emitted photon [54]. The detection of such mono-photon event can be made with the usual signature of high-p_T photon plus MET, where MET will peak around the resonance mass of the mediator.

3 Calculation of the DM relic density near a resonance

The DM abundance and, consequently, the cross sections involved in its primordial production, are typically calculated taking into account processes in equilibrium and away from poles or production resonances of a given species. When considering a resonant production processes, like the one investigated in this work, one cannot simply apply the usual solution of the Boltzmann equation in terms of $\langle\sigma v\rangle$. We address this issue by following the steps described in Ref. [30] and write $\langle\sigma v\rangle$ as a non-relativistic BW resonance (like it is the case for a cold DM candidate in the LCDM model) in the following form

$$\langle\sigma v\rangle_{\rm res} = \frac{16\pi}{m_\chi^2}\frac{(2J+1)}{(2S+1)^2}x^{3/2}\pi^{1/2}\frac{M_{Z'}\Gamma_{Z'}}{m_\chi^2}B_i(1-B_i) \times \sum_{l=0}^{\infty}\frac{b_R^{(l)}}{l!}F_l(z_R;x), \tag{10}$$

where $x = m_\chi/T$ and the quantities J and B_i are, respectively, the spin and resonance branching fraction of the initial state, whereas S and m_χ are the spin and mass of the DM particle, respectively. Here we consider the annihilation of DM particles into SM ones via the resonant mediator Z' in the relic density calculation, hence the initial state particles are the DM candidates themselves in the cosmological context of this equation. The terms $b_R^{(l)}$ are the coefficients of the expansion of a function involving the branching fraction B_i of the form

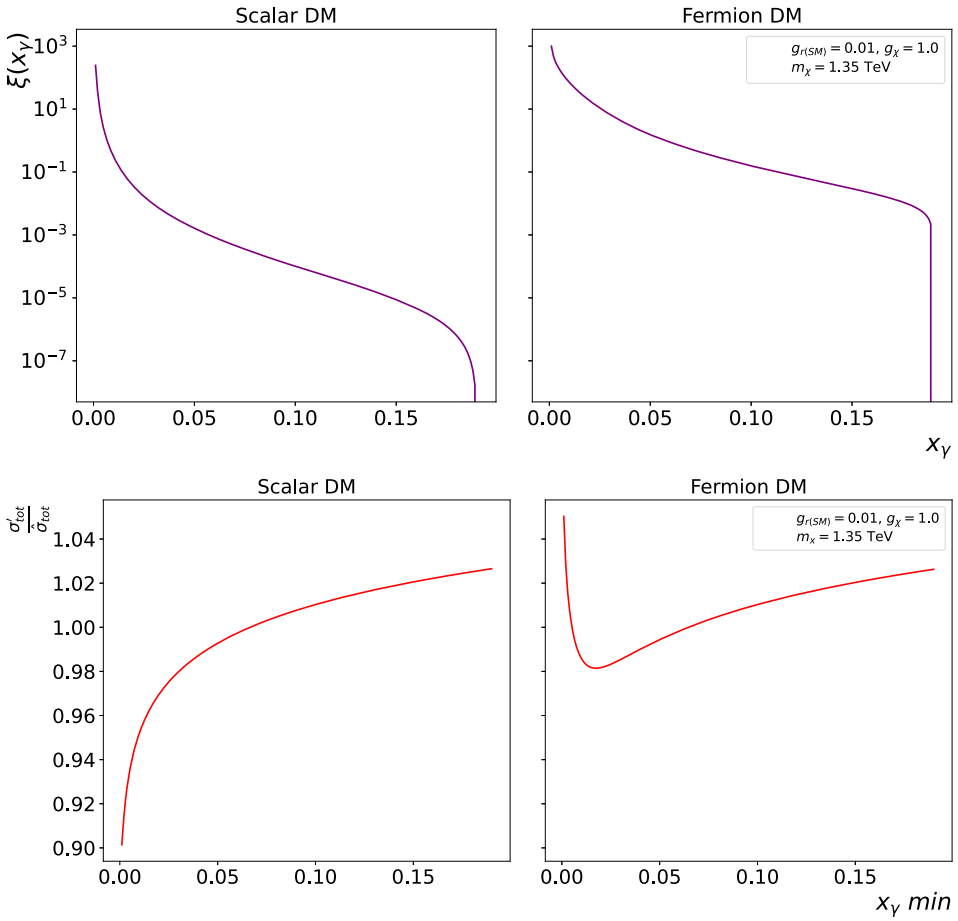

Fig. 3 (Top panel) Correction $\xi(x_\gamma)$ in terms of the photon energy fraction, which account for radiative corrections. (Bottom panel) The ratio of the cross section with ISR, $\sigma'_{\rm tot}$, and without ISR, $\hat{\sigma}_{\rm tot}$, that represents $1+\delta$ of Eq. 7 carrying all radiative corrections. In both cases the cross sections are computed with $M_{Z'} = 3$ TeV and $m_\chi = 1$ GeV

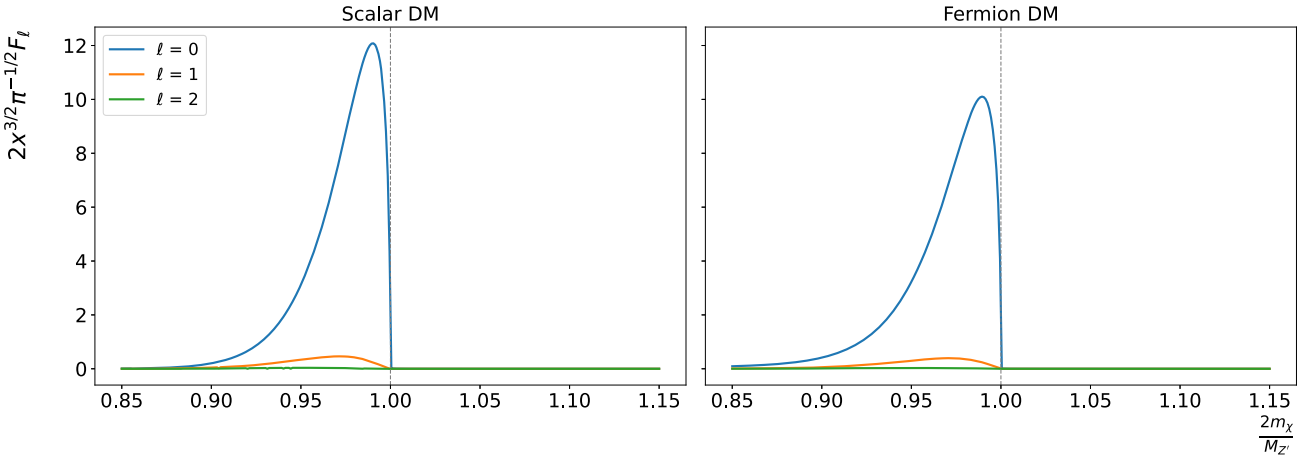

Fig. 4 Profile of the thermal average, $\Sigma(z_R; x)$, near the Z' resonance for $l = 0, 1, 2$

$$b_R(\epsilon) \equiv \frac{B_i(1-B_i)(1+\epsilon)^{1/2}}{\epsilon^{1/2}(1+2\epsilon)} = \sum_{l=0}^{\infty} \frac{b_R^{(l)}}{l!}\epsilon^l, \tag{11}$$

in terms of ϵ, which is the energy per unit mass of the process as a whole defined by

$$\epsilon = \frac{s - m_\chi^2}{m_\chi^2}. \tag{12}$$

Lastly, the $F_l(z_R; x)$ term results from the thermal average of σv with integration over the energy per unit mass ϵ

$$F_l(z_R; x) = \mathrm{Re}\frac{i}{\pi}\int_0^\infty \frac{\epsilon^{(l+1/2)}e^{-x\epsilon}}{(z_R - \epsilon)}\mathrm{d}\epsilon, \tag{13}$$

with a ϵ^l factor from Eq. 11 and an auxiliary variable in terms of the masses and decay widths of the particles involved

$$z_R = \frac{M_{Z'}^2 - m_\chi^2}{m_\chi^2} + i\frac{M_{Z'}\Gamma_{Z'}}{m_\chi^2}. \tag{14}$$

We can investigate with these results the profile of the thermal average near the resonance computed in the proper framework for the expansion of the BW cross section. As we can see in Fig. 4, the profile defined as

$$\Sigma(z_R; x) = 2x^{3/2}\pi^{-1/2}F_l(z_R; x) \tag{15}$$

shows the relative masses where the enhancement in the thermal average arises near the Z' resonance, for relative masses above 0.8. For relative masses below threshold the thermal average is very similar if compared to the usual, non-resonant calculation of the thermal average. The enhancement peak is positioned at DM masses below the resonance mass given the fact that there is enough thermal energy to produce a heavier resonance during the equilibrium phase. Also, the profile does not extend beyond the resonance mass since we are taking into account a narrow resonances for the Z' boson for both scalar and fermion DM (both $\Gamma_{Z'}/M_{Z'} \sim 10^{-2}$). DM particle with masses above the resonance mass would be possible for wider resonances, where low energy tail would allow a non-zero thermal average for DM particles with relative mass above the resonance mass. As a result, we consider in this study m_χ masses with relative mass in the range $0.8 < 2m_\chi/M_{Z'} < 1.0$ in order to probe the region where the thermal average is enhanced by the Z' resonance: together with the relic density, results will contain a (red dashed) line delimiting the threshold relative to $2m_\chi/M_{Z'} = 0.8$. Taking for instance a resonance of 3 TeV, the threshold of m_χ with enough thermal energy to produce a Z' starts at 1350 GeV – we use this mass value as reference.

Nonetheless, Eqs. 11 and 13 can be combined to express $F_l(z_R; x)$ without the expansion in l terms as

$$F(z_R; x) = \mathrm{Re}\frac{i}{\pi}\int_0^\infty \frac{(1+\epsilon)^{1/2}e^{-x\epsilon}}{(1+2\epsilon)(z_R-\epsilon)}\mathrm{d}\epsilon. \tag{16}$$

This way we can rewrite Eq. 10 in a simpler form without relying on the expansion in terms of ϵ^l as done in Ref. [30]. This, in turn, has been evaluated by means of the following expression

$$\langle\sigma v\rangle_{\mathrm{res}} = \frac{16\pi}{m_\chi^2}\frac{(2J+1)}{(2S+1)^2}x^{3/2}\pi^{1/2} \times \frac{M_{Z'}\Gamma_{Z'}}{m_\chi^2}B_i(1-B_i)\,F(z_R; x), \tag{17}$$

which allows us to numerically estimate the dimensionless density parameter referring to the primordial DM fraction as [30,40]

$$\Omega_\chi h^2 \approx 8.76\times 10^{-11}\,\mathrm{GeV}^{-2}\left[\int_{T_0}^{T_f} g_*^{1/2}\langle\sigma v\rangle_{\mathrm{res}}\frac{\mathrm{d}T}{m_\chi}\right]^{-1}, \tag{18}$$

being T_0 and T_f the current and at *freeze-out* temperatures, respectively, and g_* are the particles degrees of freedom in the same epoch.

The production process with ISR photon needs to probe the enhanced region above $\sqrt{s} = 0.8M_{Z'}$. Thus, the reduced beam energy resulting from the photon emission cannot go below this threshold if we want to investigate the mass region near the Z' resonance, restricting the photon energy for possible searches of DM production. In this work we consider a photon irradiation from an incoming fermion with energies ranging from 60 GeV up to $0.2M_{Z'}$, allowing to evaluate the production cross section where the relic density will be lesser suppressed near the resonance.

As a result of the proper calculation of the relic density with usual SM-DM and DM-DM coupling found in the literature, namely $g_\chi = 1.0$ and $g_{r/l} = 0.25$, an extension of the available parameter space is expected in comparison the usual calculation outside resonance regions (namely the "naive" approach as used by Ref. [30]). This extended region can be seen in Fig. 5 by the reduced exclusion region in contrast to the usual calculation performed by experimental searches, such as the one by the CMS Collaboration in Ref. [29], where all phase space below the blue solid line is excluded. These results are an improvement of a factor of 3–4 in g_χ and a factor ~ 2 in $g_{r/l}$ within the LHC kinematics. We note that the regions in the mass scan differ significantly from those shown in other works that do not take into account processes near or at the resonance peak of a massive mediator, even though numerically calculated for analogous processes [13,28]. This corroborates the assertion by the authors in Ref. [30] that the incorrect evaluation of resonance results in a reduction of $\langle\sigma v\rangle$, the velocity-weighted cross-section. Consequently, the naive approach overestimates the relic density and the proper calculation reduced the exclusion regions in the parameter space. These findings motivate us to investigate this approach in more detail.

Following the recommendations in the literature [13–15, 28,29,65,68–70], we opted to analyze two scenarios for each studied initial state, where the coupling of the mediator with the SM is fixed: $g_{r/l} = 0.01$ and 0.1 for the $\ell\ell Z'$ coupling in e^+e^- collisions and $g_{r/l} = 0.10$ and 0.25 for the $q\bar{q}Z'$ coupling in pp collisions, whereas the coupling of Z' with the dark sector is set at $g_\chi = 1$ for all cases.

In the case where the mediator Z' is a pure vector, we can indeed obtain a scenario where the coupling with quarks is much greater than with leptons at tree level, and the coupling with the latter occurs only through the loop mixing of Z' with the other neutral bosons of the SM. This can naturally lead to an expected ratio of ~ 0.1 between $g_{Z'\ell\ell}/g_{Z'qq}$ [13]. All these discussed scenarios and particular values tend to be highly dependent on the specifics of the model at hand. However, considering only the scenario for massive mediators on the TeV scale, we can assume larger couplings

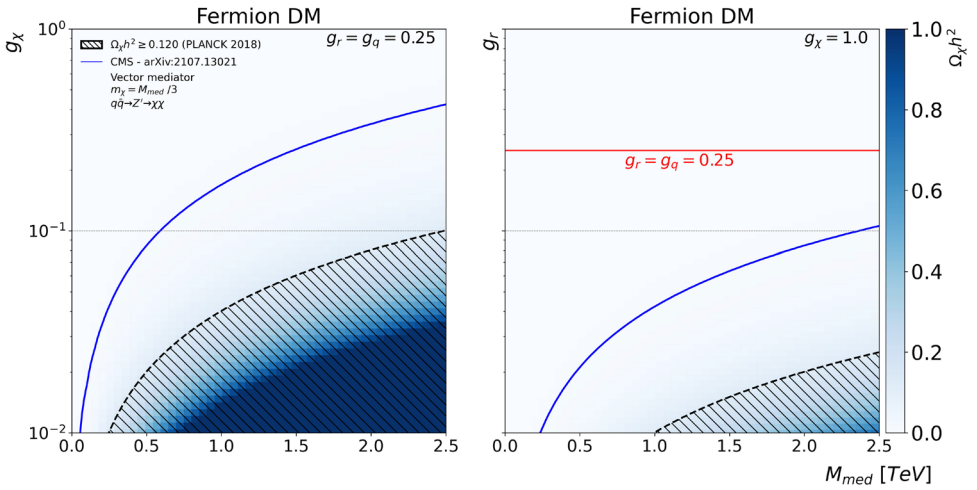

Fig. 5 Dimensionless density parameter $\Omega_\chi h^2$ for DM produced via Z' mediator with $M_{med} \equiv M_{Z'}$ [29] and DM pairs with mass $m_\chi = M_{Z'}/3$ in the s-channel taken for $q\bar{q}$ scenarios, where we scan over different values of g_r and g_χ, fixing (left panel) $g_r = 0.25$ as a leptophobic context ($g_\ell = 0$), and (right panel) $g_\chi = 1$, following Refs. [12–15,28,29,68], and overlaying the curve for the naive approach evaluated by the CMS Collaboration in Refs. [13,29]

($g_{Z'ff} \geq 0.1 \sim 0.3$) considering that one may possible evade the constraints imposed by direct and indirect detection experiments in this mass regime [6,7]. Also, larger couplings could be explored if a specific model imposes multi-TeV masses on the mediator, which would further escape direct detection constraints, particularly those related to the coupling, a significant restriction in interaction models via Z'. In general, smaller coupling values favor collider searches as they become more sensitive (as more data is collected), given the clear reduction in the magnitude of such processes. However, very low coupling values disadvantage thermal DM production scenarios, as the calculated relic abundance of such processes increases considerably [30,31].

Figures 6 and 7 show how the DM overabundance regions, behave in the mass scans $m_\chi \times M_{Z'}$, parameterized by the dimensionless density $\Omega_\chi h^2$ obtained with Eq. 18. The region that comprises the limit with $\Omega_\chi h^2 \geq 0.120$ corresponds to the hatched area and is used in all results indicating the region of excess primordial DM production. These results show that the proper calculation of these limits is essential to evaluate the available regions to probe the mass of the mediator and the DM particles taking into account the limits obtained from astrophysical observations. When the $\ell\ell Z'$ coupling is set to $g_r = 0.01$, most mass regions are largely excluded for the CLIC energy regime, as seen in the top panels of Fig. 6. However, for larger values of the g_r coupling in the bottom panels of Fig. 6, we observe a significant reduction in the area corresponding DM overabundance, which favors resonance searches in e^+e^- accelerators like CLIC and ILC [65,71,72]. This is because results from these experiments evade the limits imposed by the LHC, especially in scenarios with leptophilic models without couplings to quarks at tree-level. Similarly, the LHC kinematics shown in Fig. 7 reveals opportunities for probing new mediators, due to the area corresponding to the region excluded being quite small as well. In these cases, significantly smaller regions of the phase space are excluded for scalar DM, while remaining entirely accessible for fermion DM. Besides, the mass scan for fermion DM shows that the limits evaluated in the naive approach (below blue solid line) produce significant exclusion regions which are not really limitations if the proper calculation near a resonance is considered.

In order to verify the complete available regions in the parameter space, Figs. 8 and 9 present the scans of couplings $g_r \times g_\chi$ for both CLIC and LHC kinematics. They show very similar shapes of the exclusion regions for both DM species and coupling possibilities (as detailed in Table 1), differing mainly in terms of the exclusion area that aligns with the observed relic density, however show quite different results between e^+e^- and pp collisions. The region of overabundance for e^+e^- collisions seen in Fig. 6 for $g_r = 0.01$ chosen for the $\ell\ell Z'$ coupling is within the excluded region even considering the enhancement due to the resonance. On the other hand, it becomes largely accessible with varying the fermion DM and mediator masses with $g_r = 0.1$ and very restricted for scalar DM, inaccessible at CLIC at 3 TeV. However, larger values of the $\ell\ell Z'$ coupling need to be analyzed considering a possible leptophobic behavior of the mediator, where more restrictive limits may or may not be imposed when resonance searches in di-leptons are included [68,69]. The same does not happen for the LHC energy regime, where the $g_r = 0.1$ or $g_r = 0.25$ lies close to but above the limit of overabundance of the relic density and largely accessible within the current collider experiments. As already mentioned, the mediator is

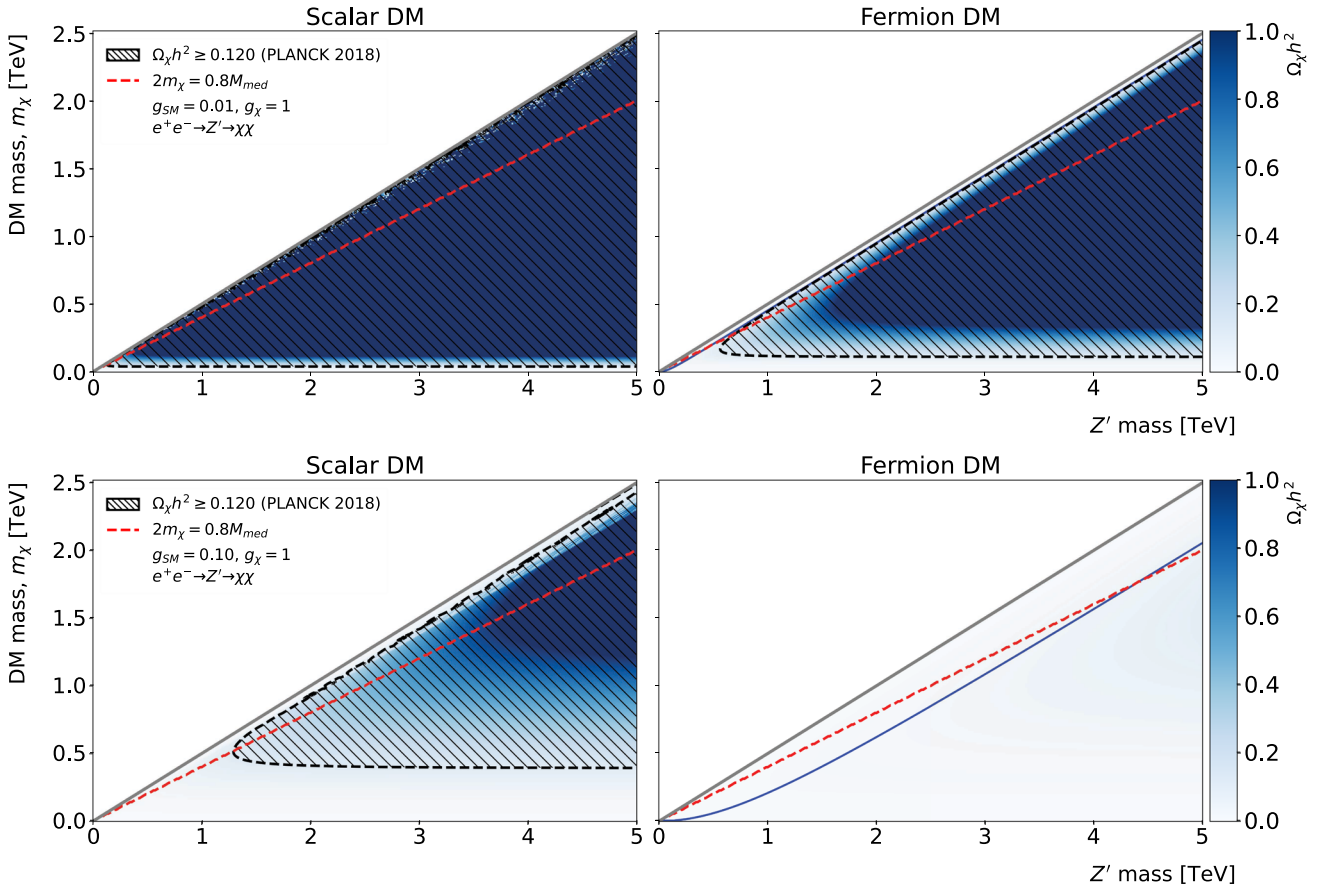

Fig. 6 Dimensionless density parameter $\Omega_\chi h^2$ for DM produced via Z' mediator with mass $M_{Z'}$ and DM pairs with mass m_χ taken for e^+e^- collisions, whereas a Z' couples with all six SM leptons pairs ($N_f = 6$) in the final state. The hatched area shows the regions with DM overabundance compared to the observed CDM abundance, which are excluded. The diagonal solid line represents the kinematic limit with $m_\chi = M_{Z'}/2$. For the upper plot, $g_r = 0.01$ and $g_\chi = 1$, while $g_r = 0.1$ and $g_\chi = 1$ for the bottom one. The red dashed lines show the threshold of the m_χ to produce the resonance with thermal energy while the blue solid lines on the fermion DM plots indicate the naive approach for relic density calculations, as in Ref. [13], i.e., line for $\Omega_\chi h^2 = 0.120$ with all region below the line being excluded

independent, and its coupling is restricted either with leptons or with quarks, then limits in searches for resonances with di-leptons do not directly apply. We shall stress here the fact that the calculation with the proper evaluation of the relic density near a resonance has produced shorted limitations in the parameter space, especially in the LHC energy regime as seen in Fig. 9. These results show that the limits imposed on the mass of the potential spin-1 mediator by analyses of the data from LHC experiments should take it properly into account.

4 Results and discussion

The DM production is very distinctive between lepton and hadron colliders given the available beam energies and detector coverage. We investigate the feasibility of DM production at CLIC and the LHC considering the calorimeter detectors planned/available for photon isolation and reconstruction. The production of DM may be detected by the emission of SM particles in an initial interaction state, where only SM particles and its respective couplings are involved [12,14]. Searches known as *mono-X* may indicate the associated production of jets, vector bosons (H,Z), photons, among others as initial state radiations (ISR). For instance, the future experiments at CLIC will be especially sensitive to wide searches of DM in mono-photon production [65]. In this work we investigate the DM production rates over scalar and fermion DM final states, where a massive mediator acts as a portal with the dark sector in s-channel processes with mono-photon ISR at high-energy colliders.

Hence, we scan the parameter space and find exclusion regions based on the relic density abundance, which shows possible scenarios in the dark sector by means of the sensibility for different species of DM particles. One of the advantage of using particle colliders for the DM searches is that detec-

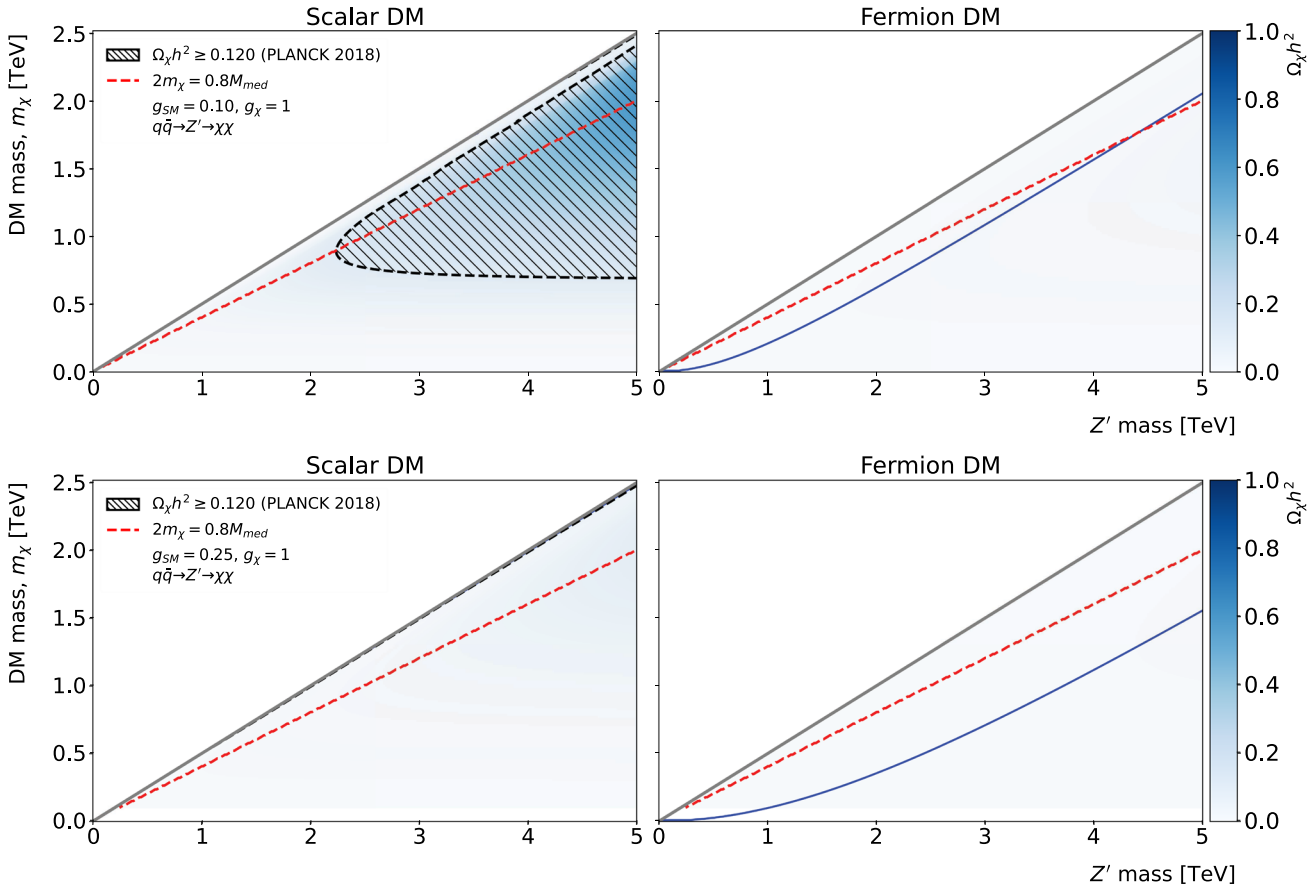

Fig. 7 Same as Fig. 6, but with Z' coupling to quark only ($N_f = 18$) as final states and with a $g_r = 0.10$ (top panel) and $g_r = 0.25$ (bottom panel)

tors may be designed to be *multipurpose*, that is, they make it possible to measure a large number of observables within the expected production processes. Furthermore, the high integrated luminosity ($\int \mathcal{L}dt$) achieved in such colliders reduce the statistical uncertainties for the search of evidence of New Physics. This huge number of events comes together, however, with a large number of background events, but may be subtracted from experimental data with a set of selection criteria and good control of uncertainties and systematic errors, which can be simulated and studied separately [3].

4.1 Kinematics in lepton and hadron colliders

We start investigating the partonic cross section of DM particle production (Eq. 3) in e^+e^- annihilation at CLIC [71,73] at $\sqrt{s} = 3$ TeV and next pp collisions at the LHC at $\sqrt{s} = 14$ TeV, with the initial state fermion mass $m_\psi = m_e$ and $m_\psi = m_q$, respectively. The predictions for CLIC are straightforward given the beam-beam annihilation and resonance production. The mono-photon production in e^+e^- collisions is obtained by the convolution of the partonic cross section and the ISR photon,

$$\sigma'_{\rm tot}(e^+e^- \to Z'\gamma \to \gamma\chi\bar{\chi}) = \hat{\sigma}_{\rm tot}(\psi\bar{\psi} \to Z' \to \chi\bar{\chi})(1+\delta), \tag{19}$$

with δ given by Eq. 8. On the other hand, one needs to employ collinear factorization for a typical Drell–Yan-like process to evaluate the cross section in pp collisions, as shown in Fig. 10. In this framework we have for the cross section given by

$$\sigma_{\rm tot} = \int_0^1 \int_{\tau/x_1}^1 P_{q,\bar{q}}(x_1, x_2)\hat{\sigma}_{\rm tot}(q\bar{q} \to Z' \to \chi\bar{\chi}) \times \delta(\tau s - M_{Z'}^2)\, {\rm d}x_2 {\rm d}x_1, \tag{20}$$

where x_i are the longitudinal momentum fractions of the proton carried by the partons with $\tau = x_1x_2 = M_{Z'}^2/s$ and

$$P_{q,\bar{q}}(x_1, x_2) = \sum_{q=1}^{N_f} \Big[f_q(x_1, Q^2) f_{\bar{q}}(x_2, Q^2) + f_{\bar{q}}(x_1, Q^2) f_q(x_2, Q^2) \Big], \tag{21}$$

is the probability that each quark has a fraction x_i of the total proton momentum. In this work we use the parametrization

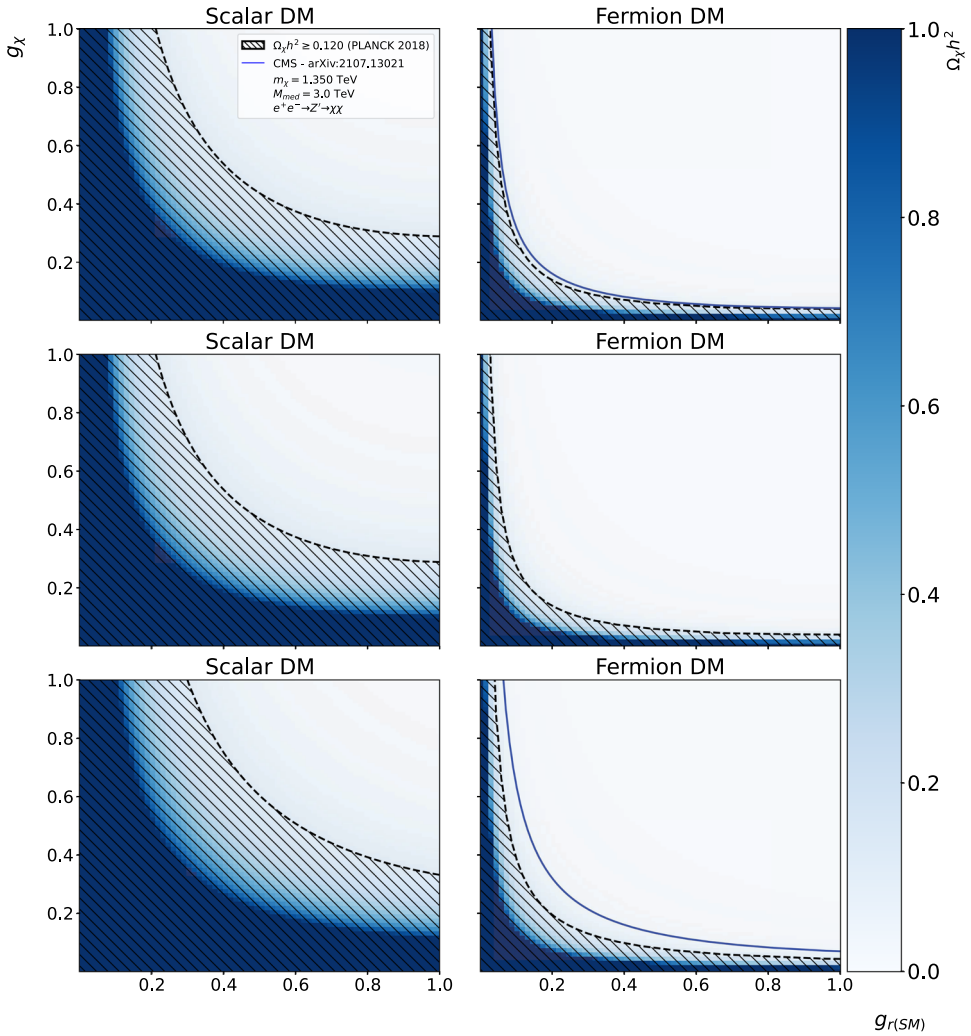

Fig. 8 Dimensionless density parameter $\Omega_\chi h^2$ for DM produced by a resonance with mass $M_{Z'} = 3$ TeV and decaying into DM pairs of mass 1350 GeV, whereas a Z' couples with all six SM leptons pairs ($N_f = 6$) in the final state. The results shown here were obtained using Eq. 18. The region with a cross section smaller than that needed to produce the observed CDM abundance is shown beveled in black. We have vector couplings in the first row, axial-vector couplings in the second, and chiral (right) in the third one

`NNPDF31_lo_as_0118` [74] to model the parton density functions (PDF) within `LHAPDF` [75], where we consider contributions from u, d, and s quarks. Considering that we are interested in the cross section near the resonance, we can write the hadronic cross section as function of τ, such as

$$M^2 \frac{\mathrm{d}\sigma}{\mathrm{d}M^2}\bigg|_{M=M_{Z'}} = \tau \int_\tau^1 f_q(x_1, Q^2) f_{\bar{q}}(\tau/x1, Q^2) \hat{\sigma}_{\mathrm{tot}}(\tau s) \times \frac{\mathrm{d}x_1}{x_1}, \tag{22}$$

with the mass fixed at the dark mediator mass.

The production cross section in pp collisions needs to incorporate the photon ISR within the partonic cross section $\hat{\sigma}_{\mathrm{tot}}$ given that the momentum loss by the quark after the photon emission has to be taken into account. Thus, the corresponding production cross section in pp collisions has the form:

$$\sigma'_{\mathrm{tot}}(pp \to Z'\gamma \to \gamma\chi\bar{\chi}) \equiv M^2 \frac{\mathrm{d}\sigma}{\mathrm{d}M^2}\bigg|_{M=M_{Z'}} = \tau \int_\tau^1 f_q(x_1, Q^2) f_{\bar{q}}(\tau/x_1, Q^2) \hat{\sigma}'_{\mathrm{tot}}(\tau s) \frac{\mathrm{d}x_1}{x_1}, \tag{23}$$

$$\hat{\sigma}'_{\mathrm{tot}}(q\bar{q} \to Z'\gamma \to \gamma\chi\bar{\chi}) = \hat{\sigma}_{\mathrm{tot}}(q\bar{q} \to Z' \to \chi\bar{\chi})(1+\delta). \tag{24}$$

We are interested in the SM signal coming from the mono-photon production mechanism in order to observe such an event in the electromagnetic calorimeters. Thus, the photon spectrum is the main experimental signature for searching the DM production. In Fig. 11 we show the normalized differential cross section for both e^+e^- and pp collisions as function of the photon energy fraction for both DM species considered in this work. One can clearly see that the fermion DM case produces a harder photon spectrum than the scalar

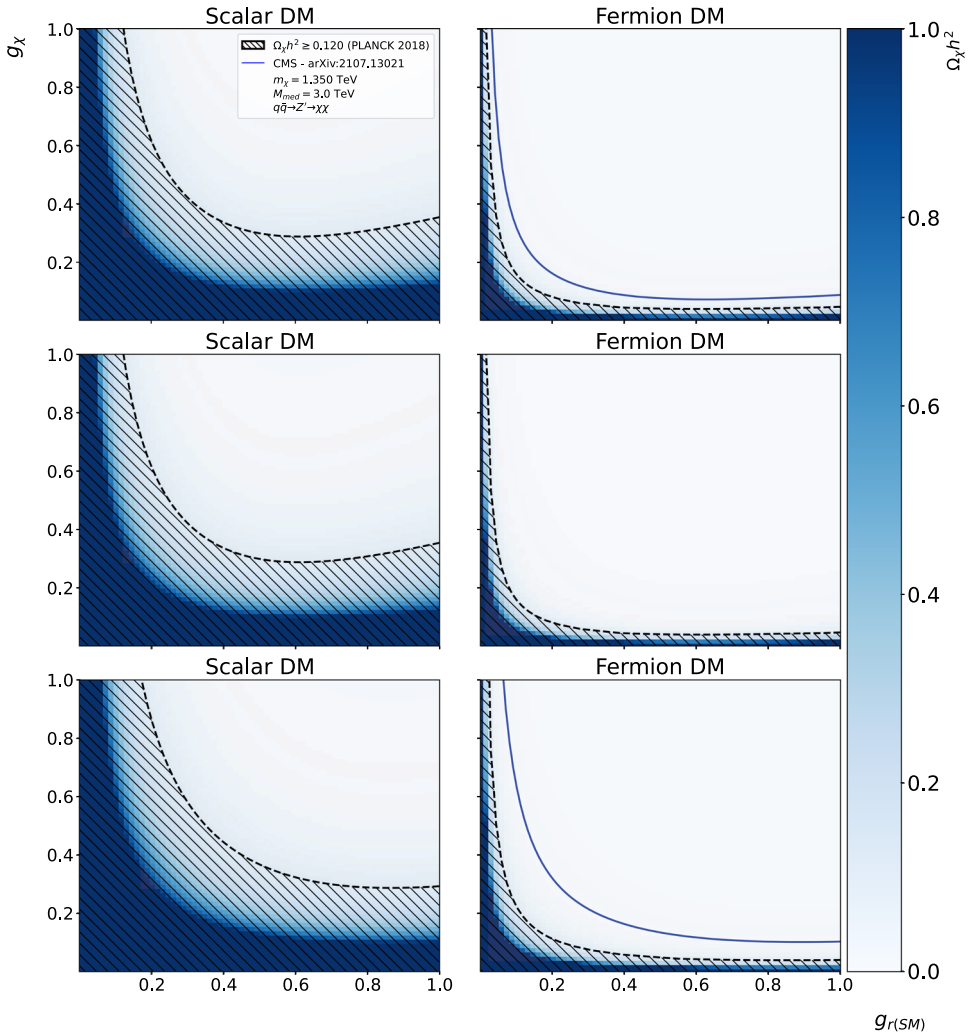

Fig. 9 Same as Fig. 8, but with Z' coupling solely with quark pairs ($N_f = 18$) as final states

DM case within the photon energy range near the resonance, which could be a hint for DM production as a experimental signature. Beyond 0.1 the normalized cross section tends to 1.

4.2 DM parameter scan

As we are mainly interested in the DM observation via production by resonances in the s-channel, Figs. 12 and 13 show the mass scan in terms of the DM production near the mediator resonance of mass $M_{Z'}$ decaying into DM particles of mass m_χ for both e^+e^- and pp collisions. Given that CLIC will operate with a fixed energy, we scan the masses in Fig. 12 with the resonant cross section with $\sqrt{s}$ at the Z' peak at 3 TeV and varying m_χ. Besides the kinematic limit of $m_\chi \leq M_{Z'}/2$, the photon ISR restricts the growth of the cross-section with m_χ, resulting in a slightly decreasing upper bound in m_χ beyond $M_{Z'} > 3$ TeV. Instead, LHC probes different invariant masses and the cross section in Fig. 13 is then free to vary with both $M_{Z'}$ and m_χ, and the restriction imposed **by** the ISR appears as a decreasing cross section right below the diagonal for $m_\chi = M_{Z'}/2$. As stated before, the coupling of the mediator with the SM is fixed to

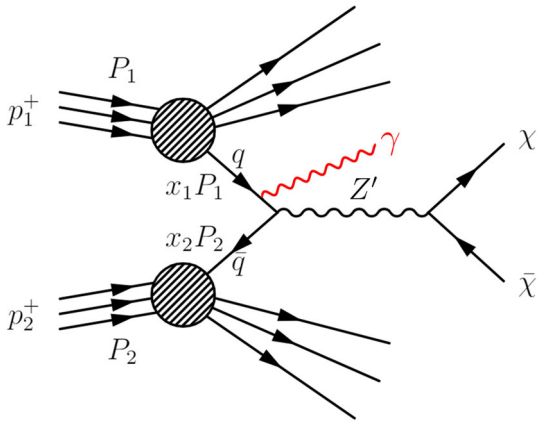

Fig. 10 A representation of a Drell–Yan-like process mediated by a massive resonance and decaying into DM final states. The same representation is used for different DM species; here shown for the fermion DM case

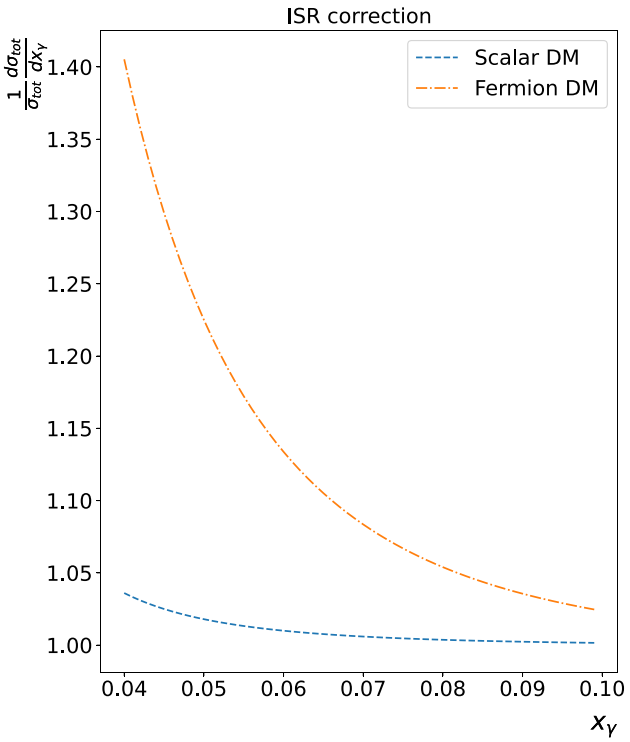

Fig. 11 Differential distributions for the ISR factorized cross section as function of the photon energy fraction, $x_\gamma = q_\gamma / E_{beam}$, normalized by the total integrated cross section. Here we use $M_{Z'} = 3$ TeV and $m_\chi = 1350$ GeV

$g_{r/l} = 0.01$ and 0.1 for the $\ell\ell Z'$ and $g_{r/l} = 0.1$ and 0.25 to $q\bar{q}Z'$ and $g_\chi = 1$ in both cases.

The hatched areas show the regions with relic overabundance and thus excluded and the red dashed line limits the region with a minimum m_χ in agreement with the relic calculation near the Z' resonance, where we note that the cross section for scalar and fermion DM are of the same order of magnitude. As we can see in Fig. 12, nearly all the mass region is excluded for the CLIC energy regime by the relic overabundance or kinematic reach for $g_r = 0.01$. Only the case of fermion DM with $g_r = 0.1$ leaves a tiny mass range available very close to the Z' peak, making it very challenging for observation at CLIC. The results for the LHC, on the other hand, show a much lesser stringent exclusion region **for** both scalar and fermion DM. Hence, the allowed region above the red dashed line results in a fully available m_χ for fermion DM and scalar DM with $g_r = 0.1$.

Considering the potential for observation at particle colliders, if any, one can see very distinctive possibilities within the DM species. The scalar and fermion DM have a significant cross section for smaller m_χ and $M_{Z'}$ masses. However, according to Refs. [28,29], massive mediators in the region below 2 TeV are already excluded with a 95% confidence level, which favors searches for regions of even higher masses. Besides, a reasonable prediction for the number of expected events needs to take into account the efficiency of identifying invisible final states and the impact of background signals, which are neglected in this work given the specifics of each detector. Hence, the observed event rate will be reduced from these predictions, but still competitive for observation, especially at the High-Luminosity LHC.

The predicted cross section for scalar and fermion DM in both e^+e^- and pp collisions resides at $\sim 10^1$–10^3 fb, which would be reduced considering detector efficiencies and background rejection to the level applied in current data analyses, however the expected event rate would be still consistent with the lack of observation as reported by the LHC experiments. Furthermore, in the spectrum chosen for the hard photon emitted as ISR, we noticed little variation in the absolute values of the cross section despite the fact that there is an evident kinematic constraint near the limit $M_{Z'} = 2m_\chi$, which indicates that, even in the case of a higher order process, this ends up not disfavoring possible future observations.

The regions not excluded by the relic density in both e^+e^- and pp collisions are very distinct and at very much different scales. Regions of DM production consistent with cosmological observations are strongly excluded for scalar DM due to the very nature of the resonant production process applied here according to Ref. [30]. This can be seen in the e^+e^- collisions at CLIC, while the restriction is much less stringent in pp collisions. Besides, regions of low DM mass are not accessible in e^+e^- collisions – neglecting the low m_χ masses far from the resonance region –, the pp ones can access the higher DM mass region at TeV scale. The cross section, and correspondingly the event rate, is comparable within the scalar and fermion DM, excluding a tiny region at higher DM mass in the scalar DM case, however this exclusion region depends on the range of photon energy which drives how DM mass in reachable in particle colliders.

Figures 14 and 15 present the distributions in terms of g_r and g_χ couplings with conventional matter and the dark sector for e^+e^- and pp collisions taking into account the photon ISR. We show the cross sections with mediator mass of $M_{Z'} = 3$ TeV and DM mass of $m_\chi = 1350$ GeV so that we are able to see more clearly the regions where the DM mass near the resonance allows the DM relic abundance production to conform with cosmological limits. We can notice that a large part of the phase space for scalar DM is excluded by the relic density, while the fermion DM is the one that presents the best observation opportunity due to its higher cross section. In addition, we see a small effect by changing the type of coupling between the SM particles and the dark mediator due to the small contribution of the coupling constants in the cross sections. One can noticed that the chiral coupling results in a slightly larger exclusion region given the nature of the g_l coupling in the cross sections and decay widths.

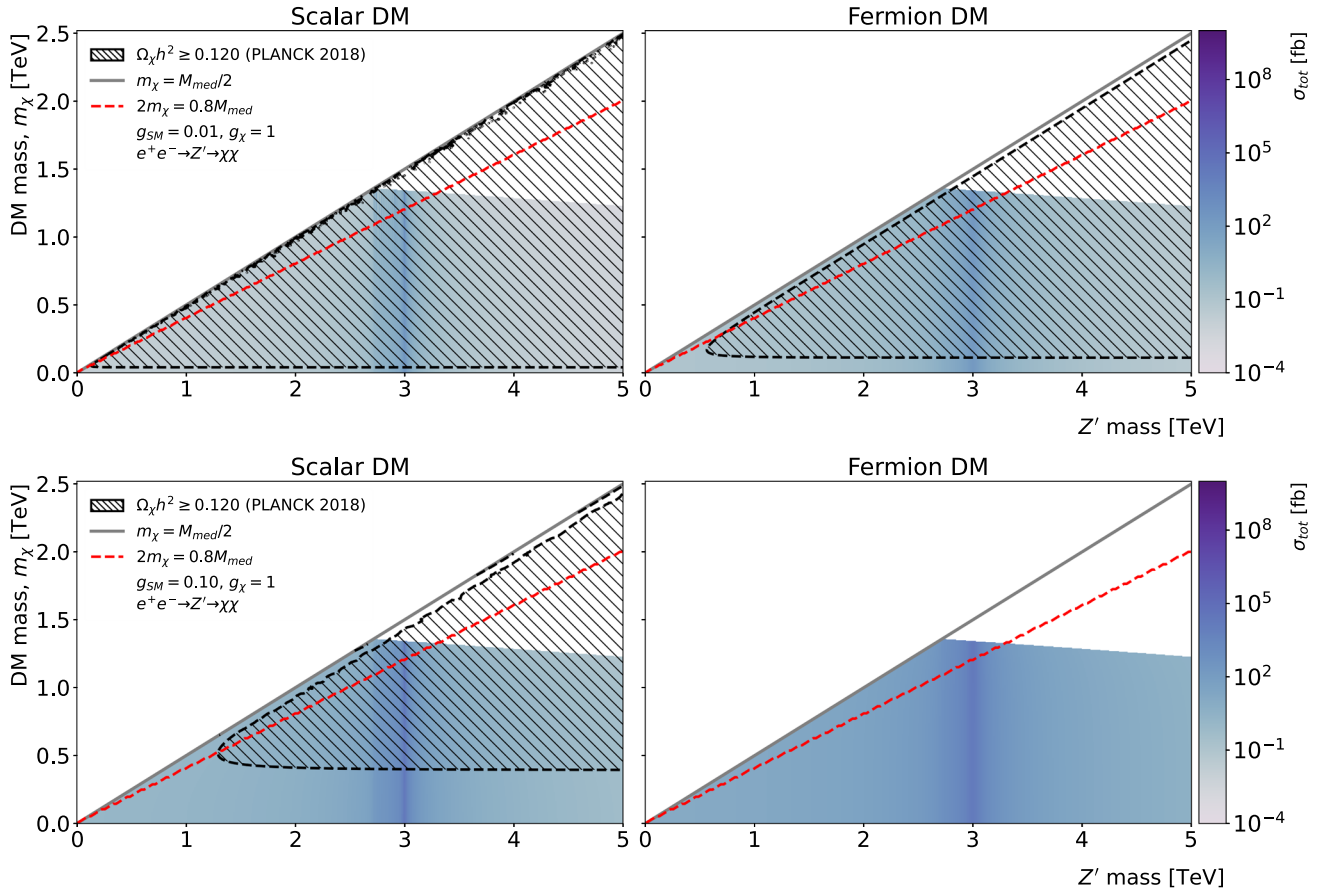

Fig. 12 Scan of the total cross section with ISR contribution as a function of the DM particle mass m_χ and mass of the mediator $M_{Z'}$ for e^+e^- collisions at CLIC at 3 TeV. The top panel illustrates the Z' coupling with the SM as $g_r = 0.01$ while the bottom panel shows the results for $g_r = 0.1$. The red dashed line draws the threshold for probing the mass range near the Z' resonance where the relic density is lesser suppressed as result of this work

5 Conclusion

We present a simplified SM extension with a new renormalizable symmetry group $U_\chi(1)$ acting as a (axial)vector portal for dark sector, which can be distinguished by the composition of its fields, i.e., scalar or fermion, by two respective possible interaction Lagrangians. We evaluated the relic density near this resonance of the Z' mediator for the first time in the literature, which drives the exclusion regions in the mass and parameter scans. As a result, we are able to define a region where the relic density is lesser suppressed, providing proper exclusion limits for DM production mediated by a Z' vector boson at TeV scale, showing that our simplified model are within the parameter space probed in the experimental and cosmological limits, excluding a significant region of coupling constants.

In this work we show that the potential for DM observation in e^+e^- collisions is very challenging, with a tiny region of the phase space still available for fermion DM very close to the resonance in case DM has a $\mathcal{O}(10^{-1})$ coupling to SM leptons. For pp collisions we can see that there is still a promising region for detection of resonances that can serve as a portal for the DM production, especially for fermion DM as a candidate in the LHC energy regime under these assumptions. Our calculation of the relic density near a resonance region is an important factor for obtaining predictions for the LHC and we showed that there still available regions for this resonance production in agreement with cosmological and collider constraints. We show that the enhancement of $\langle \sigma v \rangle$ near a resonance shrinks the exclusion regions in the parameter space when this calculation is carried out with the appropriate approach, extending the accessible coupling constants by a factor 2–4, especially at the LHC kinematic regime. This result demonstrate the experimental limits imposed on the DM mediator mass could be improved in comparison to the naive calculation of the relic density. This work aims to further narrow the parameter space, especially the mass range of the mediator mass, to establish grounds for the search of massive mediators in the resonant s-channel production. The search for New Physics, specifically the production of DM in pp colliders, is promising, even in regions already covered

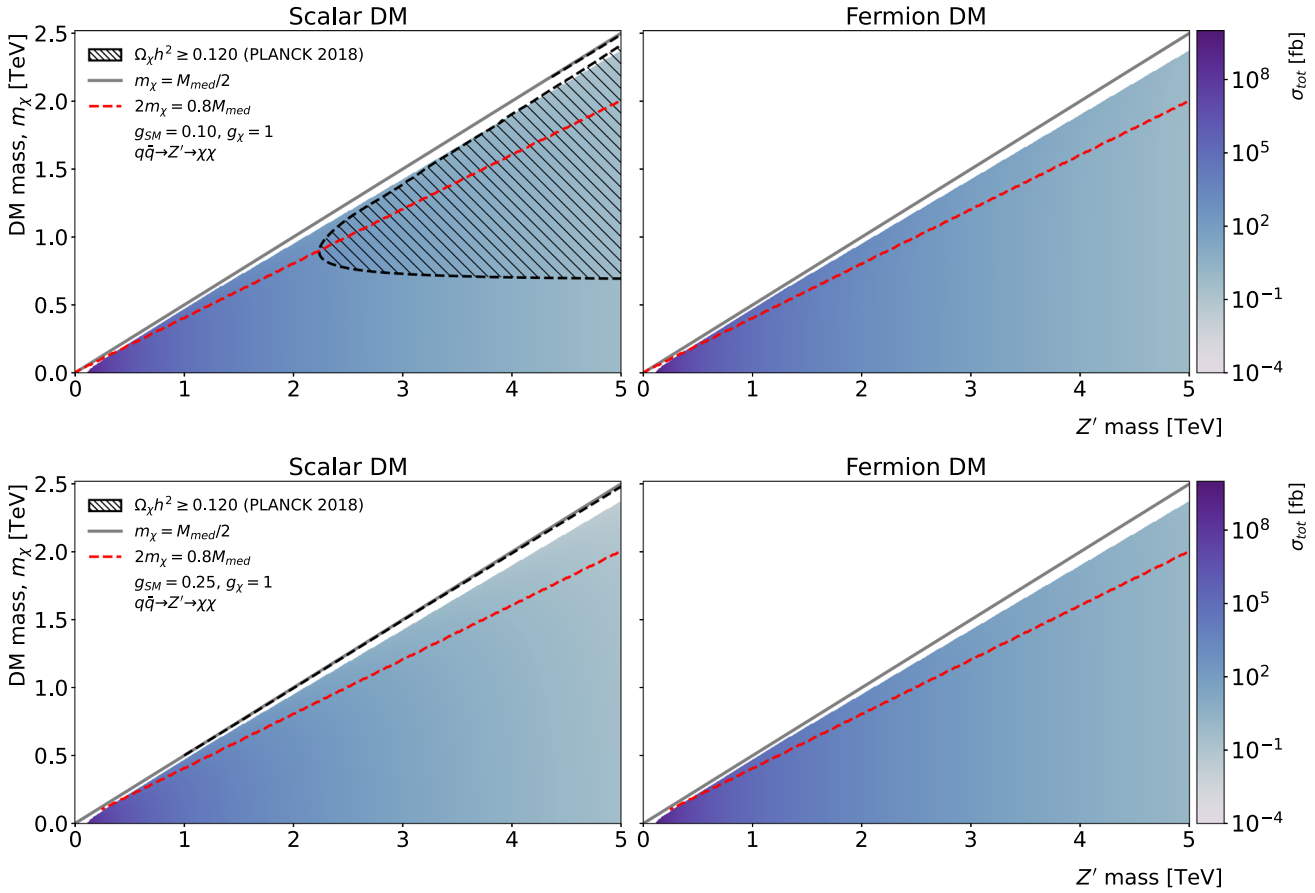

Fig. 13 Same as Fig. 12, but for pp collisions at the LHC at 14 TeV and $g_r = 0.1$ (top) and $g_r = 0.25$ (bottom)

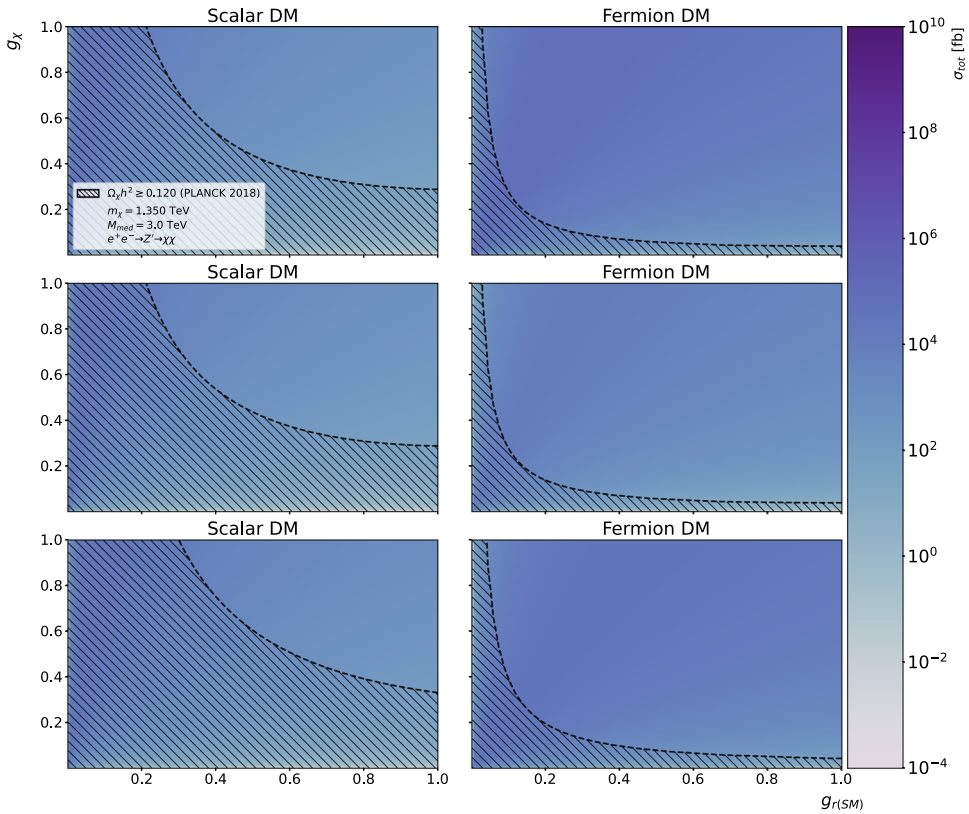

Fig. 14 Parameter scan showing the total cross section in e^+e^- collisions at CLIC at 3 TeV for each type of coupling with the SM: vector (top), axial-vector (middle), and chiral (bottom panel). The DM particle mass and the mediator mass are fixed to $m_\chi = 1350$ GeV and $M_{Z'} = 3$ TeV, respectively

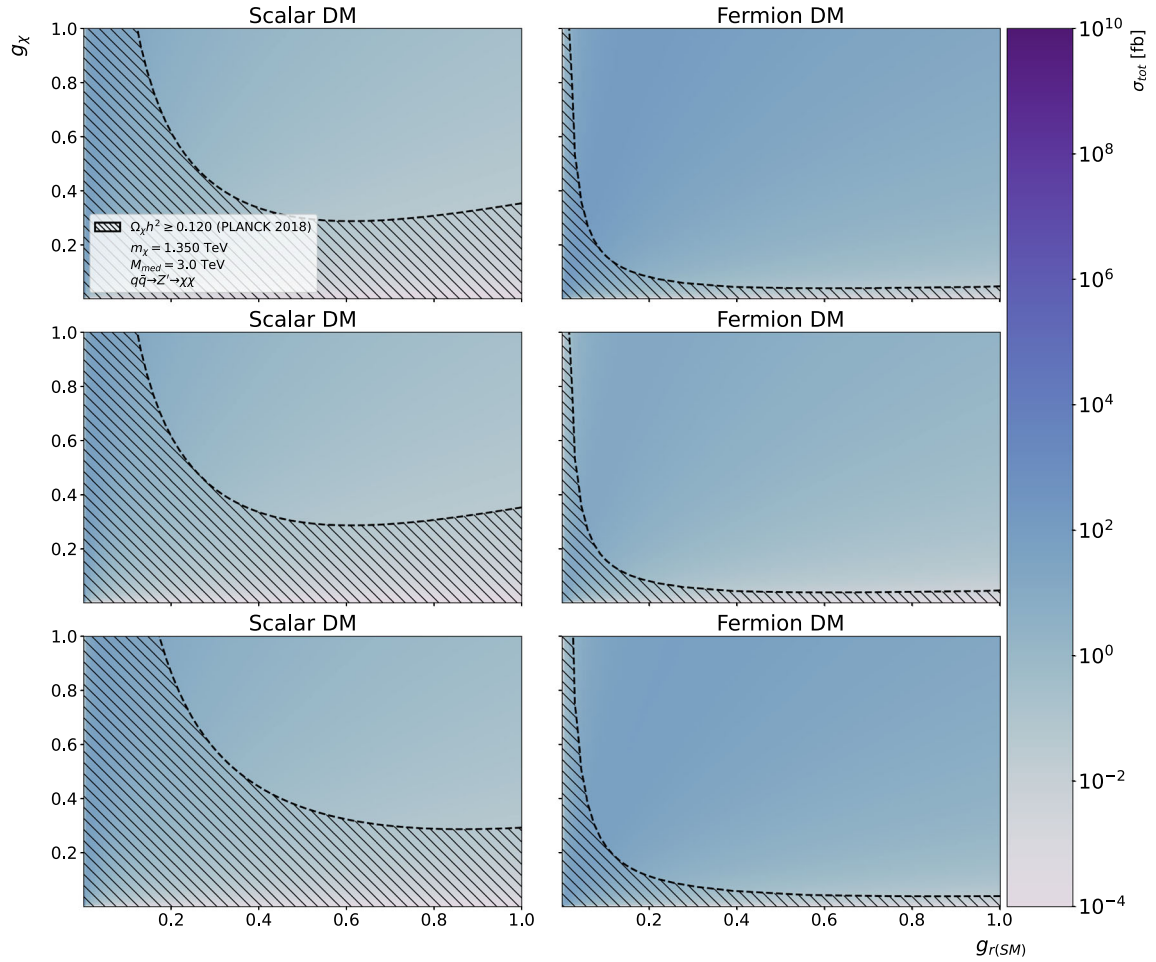

Fig. 15 Same as Fig. 14, but in *pp* collisions at the LHC at 14 TeV

by the energy and luminosity of the LHC as well as in future accelerators.

Differently from what happens in direct and indirect searches, if any DM trace have been detected in collider experiments, it would not be possible to state that the observed DM would be the same that has its gravitational effects observed at cosmological levels. This is because the time of flight of a particle to traverse all detector dependencies is not comparable to the cosmological lifetime of a stable primordial DM particle. In addition, cross-analysis of data from different experiments almost always takes some dependence on specific DM models, due to the difficulty of comparing such results independently [1,76]. The experimental viability of DM observation through these processes are focused in the use of disappearing tracks, as already done by the experiments at the LHC [77]. Therefore, our results show that searches of mono-photon production with large missing energy can be a competitive experimental signature for observing evidence of DM particles at the LHC, with the potential of characterizing the nature of a DM vector mediator in production near its resonance.

Acknowledgements This work was partially financed by the Brazilian funding agencies FAPERGS, CAPES and CNPq. This study was financed in part by the Coordenação de Aperfeiçoamento de Pessoal de Nível Superior – Brasil (CAPES) – Finance Code 001. GGS acknowledges funding from the Brazilian agency Conselho Nacional de Desenvolvimento Científico e Tecnológico (CNPq) with grant CNPq/311851/2020-7.

Data Availability Statement This manuscript has no associated data or the data will not be deposited. [Authors' comment: This is a phenomenological study and has no experimental data associated to it.]

Open Access This article is licensed under a Creative Commons Attribution 4.0 International License, which permits use, sharing, adaptation, distribution and reproduction in any medium or format, as long as you give appropriate credit to the original author(s) and the source, provide a link to the Creative Commons licence, and indicate if changes were made. The images or other third party material in this article are included in the article's Creative Commons licence, unless indicated otherwise in a credit line to the material. If material is not included in the article's Creative Commons licence and your intended use is not permitted by statutory regulation or exceeds the permitted use, you will need to obtain permission directly from the copyright holder. To view a copy of this licence, visit http://creativecommons.org/licenses/by/4.0/.
Funded by SCOAP[3].

References

1. R.L. Workman et al., Review of particle physics. PTEP **2022**, 083C01 (2022). https://doi.org/10.1093/ptep/ptac097
2. G. Bertone, D. Hooper, J. Silk, Particle dark matter: evidence, candidates and constraints. Phys. Rep. **405**, 279–390 (2005). https://doi.org/10.1016/j.physrep.2004.08.031
3. M. Bauer, T. Plehn, *Yet Another Introduction to Dark Matter: The Particle Physics Approach. Lecture Notes in Physics*, vol. 959 (Springer, Berlin, 2019). https://doi.org/10.1007/978-3-030-16234-4
4. M. Klasen, K. Kovarik, S. Schmiemann, Direct detection of neutralino dark matter with DM@NLO. PoS **EPS-HEP2017**, 068 (2017). https://doi.org/10.22323/1.314.0068
5. M. Duerr, K. Schmidt-Hoberg, S. Wild, Self-interacting dark matter with a stable vector mediator. JCAP **09**, 033 (2018). https://doi.org/10.1088/1475-7516/2018/09/033
6. M. Schumann, Direct detection of wimp dark matter: concepts and status. J. Phys. G **46**(10), 103003 (2019). https://doi.org/10.1088/1361-6471/ab2ea5
7. C.P. de los Heros, Status, challenges and directions in indirect dark matter searches. Symmetry **12**(10), 1648 (2020). https://doi.org/10.3390/sym12101648
8. R. Catena, L. Covi, SUSY dark matter(s). Eur. Phys. J. C **74**, 2703 (2014). https://doi.org/10.1140/epjc/s10052-013-2703-4
9. G. Arcadi, A. Djouadi, M. Raidal, Dark matter through the Higgs portal. Phys. Rep. **842**, 1–180 (2020). https://doi.org/10.1016/j.physrep.2019.11.003
10. D. Schmeier, Effective models for dark matter at the international linear collider (2013). https://doi.org/10.48550/arXiv.1308.4409
11. P. Agrawal, Z. Chacko, C. Kilic, R.K. Mishra, A classification of dark matter candidates with primarily spin-dependent interactions with matter. UMD-PP-10-004, RUNHETC-2010-07 (2010). arXiv:1003.1912 [hep-ph]
12. J. Abdallah et al., Simplified models for dark matter searches at the lhc. Phys. Dark Universe **9–10**, 8–23 (2015). ISSN:2212-6864. https://doi.org/10.1016/j.dark.2015.08.001
13. A. Albert et al., Recommendations of the LHC Dark Matter Working Group: comparing LHC searches for dark matter mediators in visible and invisible decay channels and calculations of the thermal relic density. Phys. Dark Universe **26**, 100377 (2019). https://doi.org/10.1016/j.dark.2019.100377
14. D. Abercrombie, N. Akchurin, E. Akilli et al., Dark matter benchmark models for early LHC run-2 searches: report of the ATLAS/CMS dark matter forum. Phys. Dark Universe **27**, 100371 (2020). ISSN:2212-6864. https://doi.org/10.1016/j.dark.2019.100371
15. A. Boveia et al., Recommendations on presenting LHC searches for missing transverse energy signals using simplified s-channel models of dark matter. Phys. Dark Universe **27**, 100365 (2020). https://doi.org/10.1016/j.dark.2019.100365
16. E.W. Kolb, M.S. Turner, *The Early Universe*, vol. 69 (CRC Press, Boca Raton, 1990). ISBN:978-0-201-62674-2. https://doi.org/10.1201/9780429492860
17. P. Langacker, The physics of heavy Z' gauge bosons. Rev. Mod. Phys. **81**, 1199–1228 (2009). https://doi.org/10.1103/RevModPhys.81.1199
18. M. Frank, K. Huitu, S. Mondal, Dark matter and collider signals in supersymmetric $U(1)'$ models with non-universal Z' couplings. Phys. Rev. D **100**(11), 115018 (2019). https://doi.org/10.1103/PhysRevD.100.115018
19. O. Buchmueller, M.J. Dolan, S.A. Malik, C. McCabe, Characterising dark matter searches at colliders and direct detection experiments: vector mediators. JHEP **01**, 037 (2015). https://doi.org/10.1007/JHEP01(2015)037
20. A. Boveia, C. Doglioni, Dark matter searches at colliders. Annu. Rev. Nucl. Part. Sci. **68**, 429–459 (2018). https://doi.org/10.1146/annurev-nucl-101917-021008
21. A.M. Sirunyan et al., Search for new physics in final states with an energetic jet or a hadronically decaying W or Z boson and transverse momentum imbalance at $\sqrt{s} = 13$ TeV. Phys. Rev. D **97**(9), 092005 (2018). https://doi.org/10.1103/PhysRevD.97.092005
22. A.M. Sirunyan et al., Search for narrow and broad dijet resonances in proton–proton collisions at $\sqrt{s} = 13$ TeV and constraints on dark matter mediators and other new particles. JHEP **08**, 130 (2018). https://doi.org/10.1007/JHEP08(2018)130
23. M. Aaboud et al., Search for dark matter and other new phenomena in events with an energetic jet and large missing transverse momentum using the ATLAS detector. JHEP **01**, 126 (2018). https://doi.org/10.1007/JHEP01(2018)126
24. L. Linssen, A. Miyamoto, M. Stanitzki, H. Weerts, Physics and detectors at CLIC: CLIC conceptual design report (2012). https://doi.org/10.5170/CERN-2012-003
25. K. Kadota, A. Spray, Electroweak multiplet dark matter at future lepton colliders. JHEP **02**, 017 (2019). https://doi.org/10.1007/JHEP02(2019)017
26. P.J. Fox, R. Harnik, J. Kopp, Y. Tsai, Missing energy signatures of dark matter at the LHC. Phys. Rev. D **85**, 056011 (2012). https://doi.org/10.1103/PhysRevD.85.056011
27. J. de Blas et al., The CLIC potential for new physics. CERN-TH-2018-267, CERN-2018-009-M (2018). https://doi.org/10.23731/CYRM-2018-003
28. G. Aad et al., Search for new phenomena in events with an energetic jet and missing transverse momentum in pp collisions at $\sqrt{s} = 13$ TeV with the ATLAS detector. Phys. Rev. D **103**(11), 112006 (2021). https://doi.org/10.1103/PhysRevD.103.112006
29. A. Tumasyan et al., Search for new particles in events with energetic jets and large missing transverse momentum in proton–proton collisions at $\sqrt{s} = 13$ TeV. JHEP **11**, 153 (2021). https://doi.org/10.1007/JHEP11(2021)153
30. P. Gondolo, G. Gelmini, Cosmic abundances of stable particles: improved analysis. Nucl. Phys. B **360**, 145–179 (1991). https://doi.org/10.1016/0550-3213(91)90438-4
31. K. Griest, D. Seckel, Three exceptions in the calculation of relic abundances. Phys. Rev. D **43**(10), 3191–3203 (1991). https://doi.org/10.1103/physrevd.43.3191
32. N. Aghanim et al., Planck 2018 results. VI. Cosmological parameters. Astron. Astrophys. **641**, A6 (2020). https://doi.org/10.1051/0004-6361/201833910. [Erratum: Astron. Astrophys. **652**, C4 (2021)]
33. R. Oncala, K. Petraki, Bound states of WIMP dark matter in Higgs-portal models. Part I. Cross-sections and transition rates. JHEP **06**, 124 (2021). https://doi.org/10.1007/JHEP06(2021)124
34. G. Bonneau, F. Martin, Hard photon emission in e^+e^- reactions. Nucl. Phys. B **27**, 381–397 (1971). https://doi.org/10.1016/0550-3213(71)90102-7
35. J. Wudka, *The Meaning of Anomalous Couplings*, vol. C960625 (1996). https://doi.org/10.48550/arXiv.hep-ph/9606478
36. D. Alves, Simplified models for LHC new physics searches. J. Phys. G **39**, 105005 (2012). https://doi.org/10.1088/0954-3899/39/10/105005
37. D. Abercrombie et al., Dark matter benchmark models for early LHC Run-2 searches: report of the ATLAS/CMS dark matter forum. Phys. Dark Universe **27**, 100371 (2020). https://doi.org/10.1016/j.dark.2019.100371
38. L. Roszkowski, E.M. Sessolo, S. Trojanowski, WIMP dark matter candidates and searches—current status and future prospects. Rep. Prog. Phys. **81**(6), 066201 (2018). https://doi.org/10.1088/1361-6633/aab913
39. A.C. Kopecky, A search for dark matter in the monophoton final state at CMS. PhD thesis, UC, Davis (2012)

40. G. Arcadi, M. Dutra, P. Ghosh, M. Lindner, Y. Mambrini, M. Pierre, S. Profumo, F.S. Queiroz, The waning of the WIMP? A review of models, searches, and constraints. Eur. Phys. J. C **78**(3), 203 (2018). https://doi.org/10.1140/epjc/s10052-018-5662-y
41. C.-F. Chang, X.-G. He, J. Tandean, Two-Higgs-doublet-portal dark-matter models in light of direct search and LHC data. JHEP **04**, 107 (2017). https://doi.org/10.1007/JHEP04(2017)107
42. M. Ruhdorfer, E. Salvioni, A. Weiler, A global view of the off-shell Higgs portal. SciPost Phys. **8**, 027 (2020). https://doi.org/10.21468/SciPostPhys.8.2.027
43. J.M. Cornell, S. Profumo, W. Shepherd, Dark matter in minimal universal extra dimensions with a stable vacuum and the "right" Higgs boson. Phys. Rev. D **89**(5), 056005 (2014). https://doi.org/10.1103/PhysRevD.89.056005
44. A. Boyarsky, M. Drewes, T. Lasserre, S. Mertens, O. Ruchayskiy, Sterile neutrino dark matter. Prog. Part. Nucl. Phys. **104**, 1–45 (2019). https://doi.org/10.1016/j.ppnp.2018.07.004
45. E. Aprile et al., The XENON1T dark matter experiment. Eur. Phys. J. C **77**(12), 881 (2017). https://doi.org/10.1140/epjc/s10052-017-5326-3
46. E. Aprile et al., Search for new physics in electronic recoil data from XENONnT. Phys. Rev. Lett. **129**(16), 161805 (2022). https://doi.org/10.1103/PhysRevLett.129.161805
47. A. Falkowski, S.F. King, E. Perdomo, M. Pierre, Flavourful Z' portal for vector-like neutrino Dark Matter and $R_{K^{(*)}}$. JHEP **08**, 061 (2018). https://doi.org/10.1007/JHEP08(2018)061
48. M.E. Cabrera, J.A. Casas, A. Delgado, S. Robles, R.R. de Austri, Naturalness of MSSM dark matter. JHEP **08**, 058 (2016). https://doi.org/10.1007/JHEP08(2016)058
49. V. Shtabovenko, R. Mertig, F. Orellana, FeynCalc 9.3: new features and improvements. Comput. Phys. Commun. **256**, 107478 (2020). https://doi.org/10.1016/j.cpc.2020.107478
50. T. Hahn, Generating Feynman diagrams and amplitudes with FeynArts 3. Comput. Phys. Commun. **140**, 418–431 (2001). https://doi.org/10.1016/S0010-4655(01)00290-9
51. Wolfram Research, Inc. Mathematica, Version 13.2. Champaign, IL (2022). https://www.wolfram.com/mathematica. Accessed 15 Jan 2024
52. S. Cebrián, Review on dark matter searches. J. Phys. Conf. Ser. **2502**, 012004 (2022). https://doi.org/10.1088/1742-6596/2502/1/012004
53. J. Kalinowski, W. Kotlarski, K. Mekala, P. Sopicki, A.F. Zarnecki, Dark matter searches with mono-photon signature at future e^+e^- colliders. SciPost Phys. Proc. **8**, 095 (2022a). https://doi.org/10.21468/SciPostPhysProc.8.095
54. J. Kalinowski, W. Kotlarski, K. Mekala, K. Zembaczynski, A.F. Zarnecki, New approach to DM searches with mono-photon signature. in *2022 Snowmass Summer Study* (2022). https://doi.org/10.48550/arXiv.2203.06776
55. E. Tolley, Dark matter searches with Mono-X signatures at the ATLAS experiment. PoS **DIS2016**, 107 (2016). https://doi.org/10.22323/1.265.0107
56. M. Davier, A. Hoecker, B. Malaescu, C.Z. Yuan, Z. Zhang, Reevaluation of the hadronic contribution to the muon magnetic anomaly using new $e + e \to \pi + \pi$-cross section data from babar. Eur. Phys. J. C **66**(1–2), 1–9 (2010). ISSN:1434-6052. https://doi.org/10.1140/epjc/s10052-010-1246-1
57. W. Kilian, T. Ohl, J. Reuter, Whizard-simulating multi-particle processes at LHC and ILC. Eur. Phys. J. C **71**(9) (2011). ISSN:1434-6052. https://doi.org/10.1140/epjc/s10052-011-1742-y
58. J. Blümlein, A. De Freitas, C. Raab, K. Schönwald, The $O(\alpha^2)$ initial state QED corrections to $e^+e^- \to \gamma^*/Z_0^*$. Nucl. Phys. B **956**, 115055 (2020). https://doi.org/10.1016/j.nuclphysb.2020.115055
59. B. McElrath, Invisible quarkonium decays as a sensitive probe of dark matter. Phys. Rev. D **72**(10) (2005). ISSN:1550-2368. https://doi.org/10.1103/physrevd.72.103508
60. J.P. Lees et al., Study of $e^+e^- \to p\bar{p}$ via initial-state radiation at BABAR. Phys. Rev. D **87**(9), 092005 (2013). https://doi.org/10.1103/PhysRevD.87.092005
61. V.P. Druzhinin, S.I. Eidelman, S.I. Serednyakov, E.P. Solodov, Hadron production via e^+e^- collisions with initial state radiation. Rev. Mod. Phys. **83**, 1545 (2011). https://doi.org/10.1103/RevModPhys.83.1545
62. M.N. Achasov et al., Study of the process $e^+e^- \to \eta\pi^0\gamma$ in the energy range $\sqrt{s} = 1.05 - 2.00$ GeV with the SND detector. Eur. Phys. J. C **80**(11), 1008 (2020). https://doi.org/10.1140/epjc/s10052-020-08556-w
63. A. Blondel et al., Standard model theory for the FCC-ee Tera-Z stage, in *Mini Workshop on Precision EW and QCD Calculations for the FCC Studies: Methods and Techniques. CERN Yellow Reports: Monographs*, vol. 3/2019 (CERN, Geneva, 2018). https://doi.org/10.23731/CYRM-2019-003
64. M.-S. Chen, P.M. Zerwas, Equivalent-particle approximations in electron and photon processes of higher order QED. Phys. Rev. D **12**, 187 (1975). https://doi.org/10.1103/PhysRevD.12.187
65. J.-J. Blaising, P. Roloff, A. Sailer, U. Schnoor, Physics performance for Dark Matter searches at $\sqrt{s} = 3$ TeV at CLIC using mono-photons and polarised beams (2021). https://doi.org/10.48550/arXiv.2103.06006
66. V. Khachatryan et al., Performance of photon reconstruction and identification with the CMS detector in proton–proton collisions at sqrt(s) = 8 TeV. JINST **10**(08), P08010 (2015). https://doi.org/10.1088/1748-0221/10/08/P08010
67. J. Kalinowski, W. Kotlarski, P. Sopicki, A.F. Zarnecki, Simulating hard photon production with WHIZARD. Eur. Phys. J. C **80**(7), 634 (2020). https://doi.org/10.1140/epjc/s10052-020-8149-6
68. CMS Collaboration, Search for resonant and nonresonant new phenomena in high-mass dilepton final states at $\sqrt{s} = 13$ TeV. JHEP **07**, 208 (2021). https://doi.org/10.1007/JHEP07(2021)208
69. J. Kalinowski, W. Kotlarski, K. Mekala, P. Sopicki, A.F. Zarnecki, Sensitivity of future linear e^+e^- colliders to processes of dark matter production with light mediator exchange. Eur. Phys. J. C **81**(10) (2021). ISSN:1434-6052. https://doi.org/10.1140/epjc/s10052-021-09758-6
70. A. Tumasyan et al., Search for resonant production of strongly coupled dark matter in proton–proton collisions at 13 TeV. JHEP **06**, 156 (2022). https://doi.org/10.1007/JHEP06(2022)156
71. O. Brunner et al., *The CLIC Project. Accelerator Physics (physics.acc-ph); High Energy Physics—Experiment* (hep-ex) (2022). https://doi.org/10.48550/arXiv.2203.09186
72. H. Dreiner, M. Huck, M. Krämer, D. Schmeier, J. Tattersall, Illuminating dark matter at the ILC. Phys. Rev. D **87**(7), 075015 (2013). https://doi.org/10.1103/PhysRevD.87.075015
73. D. Dannheim, P. Lebrun, L. Linssen, D. Schulte, F. Simon, S. Stapnes, N. Toge, H. Weerts, J. Wells, CLIC e^+e^- linear collider studies (2012). https://doi.org/10.48550/arXiv.1208.1402
74. R.D. Ball et al., Parton distributions from high-precision collider data. Eur. Phys. J. C **77**(10), 663 (2017). https://doi.org/10.1140/epjc/s10052-017-5199-5
75. A. Buckley, J. Ferrando, S. Lloyd, K. Nordström, B. Page, M. Rüfenacht, M. Schönherr, G. Watt, LHAPDF6: parton density access in the LHC precision era. Eur. Phys. J. C **75**, 132 (2015). https://doi.org/10.1140/epjc/s10052-015-3318-8
76. N. Trevisani, Collider searches for dark matter. Universe **4**(11), 131 (2018). https://doi.org/10.3390/universe4110131
77. A.M. Sirunyan et al., Search for disappearing tracks in proton-proton collisions at $\sqrt{s} = 13$ TeV. Phys. Lett. B **806**, 135502 (2020). https://doi.org/10.1016/j.physletb.2020.135502